Photodissociation dynamics of phosgene: New observations by applying a three-dimensional imaging technique

Tina Einfeld, Alexei Chichinin,[a] Christof Maul, and Karl-Heinz Gericke
Institut für Physikalische und Theoretische Chemie, Technische Universität Braunschweig, Hans–Sommer–Straße 10, D-38106 Braunschweig, Germany

(Received 7 September 2001; accepted 19 October 2001)

The photodissociation dynamics of $COCl_2$ has been studied by monitoring ground $Cl(^2P_{3/2})$ and spin–orbit excited $Cl^*(^2P_{1/2})$ fragments by applying a novel technique where the three-dimensional momentum vector of a single reaction product is directly determined. The photodissociation at 235 nm produces exclusively three fragments: $COCl_2+h\nu\rightarrow CO+2Cl$. The kinetic energy distributions of Cl and Cl* are bimodal and exhibit a different behavior for the different spin–orbit states. Our attention was turned to the dependence of the anisotropy parameter β on the fragment velocity which was observed for the first time. For both spin–orbit states the anisotropy parameter differs clearly for slow and fast chlorine atoms, where a pronounced change from the value ~0.7 to zero at about 20 kJ/mol is observed. Slow chlorine atoms are released isotropically and predominantly in the ground state Cl whereas fast chlorine atoms have an anisotropy parameter close to the theoretically limiting value and are distributed between ground and excited state Cl. These observations can be explained by a sequential decay where the first Cl fragment is released in a fast process characterized by the nonvanishing positive β parameter and a lifetime of $\leqslant$210 fs, whereas the second Cl fragment is released after a period which is long on a rotational time scale. A significant contribution of a symmetric mechanism can be excluded. © *2002 American Institute of Physics.* [DOI: 10.1063/1.1427072]

I. INTRODUCTION

Carbonyl compounds are known to exhibit a complex fragmentation scheme upon irradiation by ultraviolet light because of their small threshold energy with respect to three-body decay. The decay dynamics of acetone,[1] carbonyl cyanides,[2–5] acetyl halides,[6,7] and phosgene[8–10] have been investigated by almost any technique offered by modern reaction dynamics, among them nonresonant and resonance enhanced photofragment translational spectroscopy, photofragment imaging, velocity-map imaging and ultrafast spectroscopy. Earlier work is compiled in a review paper about photoinduced three-body decay.[11] Generally, when decaying into three fragments, in their first absorption bands all carbonyl compounds are observed to follow a step-wise decay mechanism where the two bonds break in two separate kinetic events.[12]

The characterization of three-body decays requires to experimentally obtain more detailed information than the investigation of the corresponding two-body process due to the increased number of degrees of freedom. In this paper a newly developed method is presented which combines the standard resonance enhanced multiphoton ionization and time-of-flight method (REMPI–TOF) with a position sensitive detector (PSD), thus enabling for the first time the observation of the full three-dimensional momentum vector of a single dissociation product along with a spectroscopic determination of its quantum state. The method has been applied to the detection of atomic chlorine fragments from the photoinduced three-body decay of phosgene ($COCl_2$).

Phosgene is a planar molecule belonging to the C_{2v} symmetry group and exhibits a broad first absorption continuum from 220 nm to 280 nm which has been assigned to the dipole-forbidden $^1A_2\leftarrow{}^1A_1$ transition.[13] The weak structure is evidence of vibrational predissociation of the excited electronic $^1A_2$ state. According to molecular orbital (MO) theory the ground state configuration is found to be

$$\underbrace{(7a_1)^2}_{\sigma(\mathrm{C-O})^2}\ \underbrace{(8a_1)^2(5b_1)^2}_{\sigma(\mathrm{C-Cl})^4}\ \underbrace{(2b_2)^2}_{\pi(\mathrm{C-O})^2}\ \underbrace{(6b_1)^2(9a_1)^2}_{n(\mathrm{O})^4}$$

$$\underbrace{(10a_1)^2(3b_2)^2(2a_2)^2(11a_1)^2(7b_1)^2(8b_1)^2}_{n(\mathrm{Cl})^{12}}$$

$$\underbrace{(4b_2)^0}_{\pi^*(\mathrm{C-O})}\ \underbrace{(9b_1)^0(12a_1)^0}_{\sigma^*(\mathrm{C-Cl})}\ \underbrace{(13a_1)^0}_{\sigma^*(\mathrm{C-O})}.$$

At 235 nm a $\pi^*_{CO}(4b_2)\leftarrow n_{Cl}(8b_1)$ excitation is expected. This leads to an increase of the bond length of C–O to be accompanied with the loss of the planar symmetry from C_{2v} to C_s.

Phosgene is known to decay into three fragments

$$COCl_2+h\nu\rightarrow CO+2Cl \tag{1}$$

when irradiated by light at 235 nm in the peak of the first absorption band.[9] The alternative two-body channels produce

[a]Permanent address: Institute of Chemical Kinetics and Combustion, 630090 Novosibirsk, Russia.

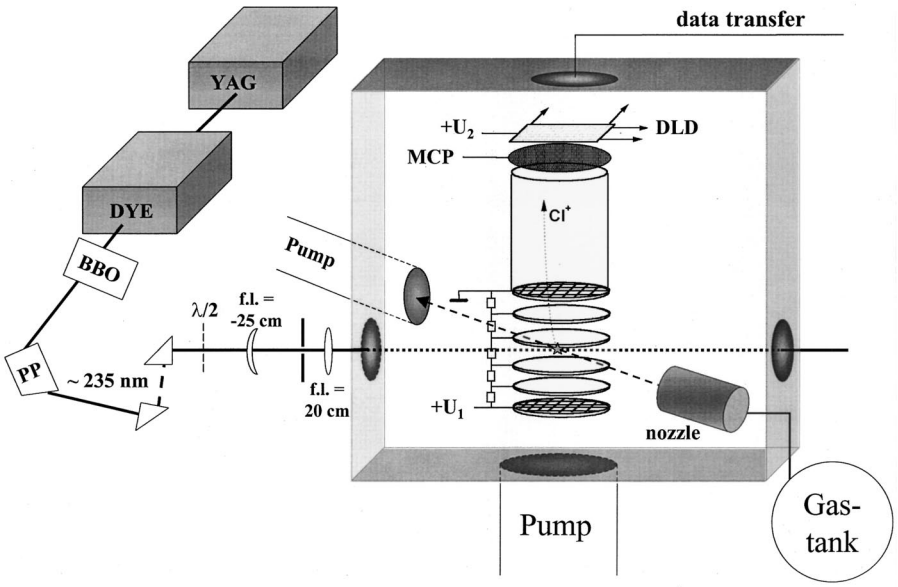

FIG. 1. A schematic REMPI/TOF/DLD 3D imaging experimental setup. BBO, frequency doubling crystal; PP, Pellin–Broca prism; λ/2, half wave plate; f.l., focal length; $+U_1$, acceleration voltage (~16 kV/m); $+U_2$, extraction voltage (~300 V); MCP, multichannel plates; DLD, delay-line detector. The photolysis and probe laser is a frequency doubled dye laser pumped by a Nd:YAG laser.

a chlorine atom and a COCl radical or a CO and a Cl_2 molecule

$$COCl_2 + h\nu \rightarrow COCl + Cl, \tag{2}$$

$$COCl_2 + h\nu \rightarrow CO + Cl_2. \tag{3}$$

At this dissociation wavelength channel (2) is not accessed and the contribution of channel (3) is small, which was derived from the analysis of the kinetic energy distributions (KED) of the partner fragments Cl and CO, respectively.[9,10] For higher dissociation energies accessing different excited electronic states emission from electronically excited Cl_2 was observed.[14] At 235 nm CO molecules are produced with a high rotational excitation resulting from the nonplanar geometry of the excited $^1A_2$ state and a nonsymmetric two-step decay mechanism.[9] Cl atoms have been monitored in both spin–orbit fine-structure states ($Cl[^2P_{3/2}]$ and $Cl^*[^2P_{1/2}]$) with a strong preference for producing ground state $Cl(^2P_{3/2})$ atoms.[10,15] The KEDs of Cl and Cl* are bimodal, but differ markedly in the contribution of slow and fast fragments.[10] These results are in accord with a nonsymmetric two-step mechanism for the three-body break-up of phosgene. A small contribution of a symmetric decay mechanism was postulated in order to fully explain the observed KEDs.

Due to the lack of experimental information about the spatial fragment distribution and about the symmetry of the excited electronic state the identity of the potential energy surface on which the dissociation proceeds has remained obscured. With our new three-dimensional imaging setup the previously observed results are fully confirmed. Additionally, the three-dimensional momentum distribution of the chlorine fragments directly yields the anisotropy parameter β, which characterizes the spatial distribution of the photofragments. For the first time the speed dependence of the β parameter is observed, allowing us to draw new conclusions on the decay mechanism and the involved potential energy surfaces.

II. EXPERIMENT

A more detailed description of the experimental setup and the novel position sensitive detector (PSD) will be published elsewhere.[16] It consists of a combination of a home-built single-field time-of-flight (TOF) mass-spectrometer and a position sensitive detector.[17–19] The spectrometer was evacuated to a base pressure of $\sim 10^{-8}$ mbar by a turbo molecular pump system. A mixture of 5% phosgene in helium was fed into the spectrometer via a continuous supersonic beam. With a nozzle diameter of 20 μm and a stagnation pressure of ca. 3 bar typical working pressures were in the order of 10^{-7} mbar. Under these conditions the beam is characterized by a rotational temperature of 8 K, determined by a rotationally resolved spectrum of the NO ($A\,^2\Sigma^+ \leftarrow X\,^2\Pi$) transition.[20]

Simultaneous dissociation and state-selective detection of chlorine atoms were performed using a single dye laser pumped by a Nd:YAG laser (Coherent, Infinity 40 100). The dye laser (Lamba Physik, Scanmate) was operated with Coumarin 47 at a repetition rate of 100 Hz, its light was frequency doubled by a BBO crystal and focussed by a 20 cm lens in order to decrease the reaction volume to 5×10^{-4} mm^3. The output window was arranged in a Brewster angle configuration of 54° to reduce the internally reflected light. The energy of the frequency-doubled light amounted to 5–10 μJ per pulse. The energy was kept low to keep the ratio of approximately one fragment signal per 10 laser pulses to avoid kinetic energy transfer to the fragments due to space charge effects and saturation of the dissociation step. The light beam, the molecular beam, and the detector axes were mutually orthogonal in the interaction region, as shown in Fig. 1. Ultimate care was taken to overlap the light and the molecular beam which was checked frequently by monitoring of NO via (1+1) REMPI at 226 nm.[20] The polarization of the laser was changed by a half wave plate in order to investigate the spatial fragment distribution. Typically the acceleration voltage was 800 V in the acceleration tube of the

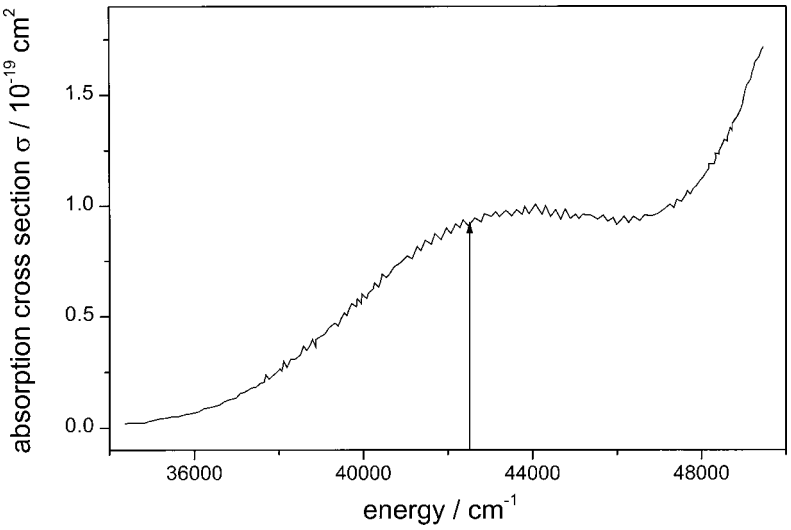

FIG. 2. Absorption cross section of $COCl_2$ based on the publication of Moule and Foo (Ref. 13). The wavelength used in the present experiment is marked by an arrow.

TOF spectrometer corresponding to an acceleration field of 16 kV/m. The ^2P_J state of the chlorine atom is split by 882 cm^{-1} due to spin–orbit coupling into $Cl(^2P_{3/2})$ and $Cl^*(^2P_{1/2})$. Both states were detected by a $(2+1)$ REMPI process. The ground state was probed via the $(^2D_{3/2} \leftarrow {}^2P_{3/2})$ transition at 235.336 nm, the excited state by the $(^2P_{1/2} \leftarrow {}^2P_{1/2})$ transition at 235.205 nm.[21,22] The $CO(X\,^1\Sigma^+)$ fragments were ionized via $(2+1)$ REMPI using the $B\,^1\Sigma^+$ state as resonant intermediate.[10,12] The employed wavelength around 230.15 nm for realizing the $(2+1)$ detection is almost at the maximum of the phosgene absorption spectrum (see Fig. 2).[13] Typically the wavelength of the Cl atom transitions was scanned over a range of ± 0.003 nm due to the Doppler broadening. Signals were processed by the electronic setup described below, digitized by time-to-digital converters (TDCs), accumulated over 2×10^5 laser shots and saved on-line by a personal computer.

The TOF spectrometer has an effective length ratio of the acceleration to the drift tube of 1:2 at a total length of 15 cm. The PSD includes a delay-line anode (DLA)[18] of the size of 100 mm$\times$100 mm introduced into the spectrometer chamber right behind the double stage multichannel plates (MCP) with an active diameter of 80 mm, as shown in Fig. 1. The DLA consists of two sets of wire pairs orthogonal to each other, one monitoring the X component and the other the Y component of the fragment momentum.[16] The individual lines of each wire pair itself are wound parallel to each other with a small inner-wire potential difference of about 30 V. An extraction voltage of about 300 V provides a collection of the charge cloud on the anode with specific broadening over several wire distances. The broad impact of the secondary electrons from the MCPs is focussed by the inner-wire potential difference. The induced signal propagates in both directions towards the ends where impedance adjusted circuits pick it up for further processing. Four differential amplifiers at the two ends of each line pair amplify only transient potential differences between the lines of a line pair, thus rejecting potential variations simultaneously present on both lines. The spatial resolution of the delay-line anode is better than 400 μm which corresponds to an energy resolution of $\sim$1% under optimal conditions.

The output charge from the MCP resulting from every single incoming ion (''event'') produces altogether four differential signals, two on each delay line pair. These signals are decoupled from the DC voltages on the wires, amplified, and transmitted to constant fraction discriminators and to the TDCs. Finally, one event produces two pairs of times, X_1, X_2 and Y_1, Y_2, on the delay lines that are wound along the X axis and the Y axis, respectively. The X and Y coordinates of a single event in time units may be calculated as (X_1-X_2, Y_1-Y_2); and the time of the event (corresponding to the Z coordinate) may be calculated as either $(X_1+X_2)/2$ or $(Y_1+Y_2)/2$. Thus the DLD yields the 3D coordinates of each single event which contain the complete information about the dissociation process. 2D images, kinetic energy distributions (KEDs), and the β anisotropy parameter can easily be extracted by appropriate averaging techniques.

III. ANALYZING PROCEDURE

From the observed 3D distributions not only the speed distribution can be extracted, but it is also possible to determine the angular distribution of the photofragments for any given speed value **v**. A general approach to study angular distributions of photodissociation products will be considered in the following. The normalized angular distribution of photofragments with a single given speed with respect to the polarization vector **E** of the electromagnetic field of the photolysis laser is usually written as

$$P(\theta,\varphi) = \frac{1}{4\pi}[1+\beta P_2(\cos\theta)]. \tag{4}$$

Here θ and φ are the polar and the azimuthal angle of the photofragment recoil velocity **v** with the polarization vector **E**, β is the anisotropy parameter which characterizes the angular distribution, and $P_2(x)$ is the second-order Legendre polynomial: $P_2(x)=\frac{1}{2}(3x^2-1)$. $P(\theta,\varphi)$ is normalized such that

$$\int_0^{\pi} \sin\theta\, d\theta \int_0^{2\pi} d\varphi\, P(\theta,\varphi) = 1.$$

If the integration over φ is performed, then a distribution $P_{\text{th}}(\theta)$ with respect to the polar angle may be defined

$$P_{\text{th}}(\theta) = \tfrac{1}{2}\sin\theta[1+\beta P_2(\cos\theta)] \tag{5}$$

such that

$$\int_0^{\pi} P_{\text{th}}(\theta)\, d\theta = 1.$$

The β parameter ranges from -1 to $+2$ with an isotropic distribution of the fragments corresponding to $\beta=0$. Most often, the β parameter is considered to be independent of the fragment velocity. However, this need not to be the case. Especially, the broader the kinetic energy distribution becomes, the more important becomes the velocity dependence of β, and the more information on the dynamics of a reaction is contained in this velocity dependence. An interesting application of the 3D technique is the study of this dependence. It means that we must calculate the β parameter for a group of photofragments that have a velocity within the range $v_0 < v < v_1$. The experimental distribution of the photofragments over the angle θ is given by the function $P_{\text{exp}}(\theta)$. The β parameter may be determined from the condition

$$\frac{\partial}{\partial\beta}\int_0^{\pi}[P_{\text{exp}}(\theta)-P_{\text{th}}(\theta)]^2\, d\theta = 0. \tag{6}$$

The normalized experimental distribution $P_{\text{exp}}(\theta)$ of the photofragments over the angle θ may be calculated as

$$P_{\text{exp}}(\theta) = \frac{1}{N}\sum_{i=1}^{N} \delta(\theta-\theta_i), \tag{7}$$

where $\delta(x)$ is a delta function, θ_i is the polar angle of the ith photofragment, and the summation is performed over particles with velocities in the range of consideration. N is the number of these particles. Inserting Eq. (7) into Eq. (6) gives the final result

$$\beta = \tfrac{4}{5}(32B_1/\pi + 1), \tag{8}$$

where

$$B_j = (1/N)\Sigma_i \sin\theta_i[P_2(\cos\theta_i)]^j.$$

The β parameter can also be obtained from a subset of the observed photofragments if the range of the angle θ is accordingly constrained. Let us determine the β parameter for a group of the photofragments that are situated in the range $a \leqslant \theta \leqslant b$. The same approach gives the final result

$$\beta = -\frac{A_0^2 B_1 - A_0(A_1B_0 + C_1) + A_1C_0}{A_0(A_1B_1 - C_2) - A_1(A_1B_0 - C_1)}, \tag{9}$$

where

$$A_j = \int_a^b [P_2(\cos\theta)]^j \sin\theta\, d\theta,$$
$$C_j = \int_a^b [P_2(\cos\theta)]^j \sin^2\theta\, d\theta.$$

Applying Eq. (8) or Eq. (9) to experimental results one can find the $\beta(v)$ dependence.

TABLE I. Limiting kinetic energies of the fragments via different decay channels.

Fragments	E_{kin} (kJ/mol) via two-body decay	E_{kin} (kJ/mol) via three-body decay
Cl	<150 >105	<105 (sequential) <80 (symmetric concerted)
CO	<290 >120	<120
Cl_2	<115	

The procedure was calibrated against the photolysis of Cl_2 at 355 nm where the perpendicular optical transition $^1\Pi_{1u} \leftarrow {}^1\Sigma_{0_g^+}$ contributes to more than 90% of the light absorption.[23–26] The excited state is repulsive, so the dissociation is fast and the β parameter must be close to its limiting value of -1. The value determined from our experimental data is $\beta = -1.00 \pm 0.05$ and agrees excellently with previous measurements and theoretical calculations.[23]

IV. RESULTS

A. Decay channels

The one-photon dissociation of phosgene can in principle proceed along one or several of the pathways (1)–(3). For a dissociation wavelength of 235 nm the following reaction enthalpies are obtained for the spin–orbit states with the lowest energy:

$$COCl_2 + h\nu \rightarrow CO + 2Cl, \qquad \Delta H(0\ \text{K}) = 344 \pm 3.5\ \text{kJ/mol},$$
$$COCl_2 + h\nu \rightarrow COCl + Cl, \qquad \Delta H(0\ \text{K}) = 274 \pm 45\ \text{kJ/mol},$$
$$COCl_2 + h\nu \rightarrow CO + Cl_2, \qquad \Delta H(0\ \text{K}) = 105 \pm 3.5\ \text{kJ/mol}.$$

The dissociation enthalpies were calculated from the standard enthalpies of formation (ΔH_f^0) (Ref. 26) of the molecules and radicals involved in the process and the errors were calculated as the square root of the sum of individual squared errors. The $\Delta H(0\ \text{K})$ required for loss of one or two Cl* atoms is higher than the values given for one or two Cl atoms in reactions (2) and (1) by 10.6 kJ/mol and 21.2 kJ/mol, respectively. The maximal kinetic energies for the fragments via the different decay channels are shown in Table I.

From the following considerations it is concluded that the radical channel (2) does not contribute to the fragmentation process of phosgene. If a stable COCl radical would be generated in the dissociation together with an atomic Cl fragment this radical would have to carry an internal energy less than its very low dissociation energy of ~70 kJ/mol.[10] Since the available energy E_{av} for the radical channel is 234 kJ/mol ($E_{\text{av}} = h\nu - \Delta H(0\ \text{K})$), the total fragment kinetic energy must be in the range from 164 to 234 kJ/mol, corresponding to a Cl kinetic energy range from 105 to 150 kJ/mol. Clearly, the Cl KED shown in Fig. 3 does not extend into this region, therefore the participation of the radical channel (2) can be ruled out confirming previous results.[10] We conclude that the dissociation process produces two chlorine atoms or molecular chlorine and one carbon monoxide molecule.

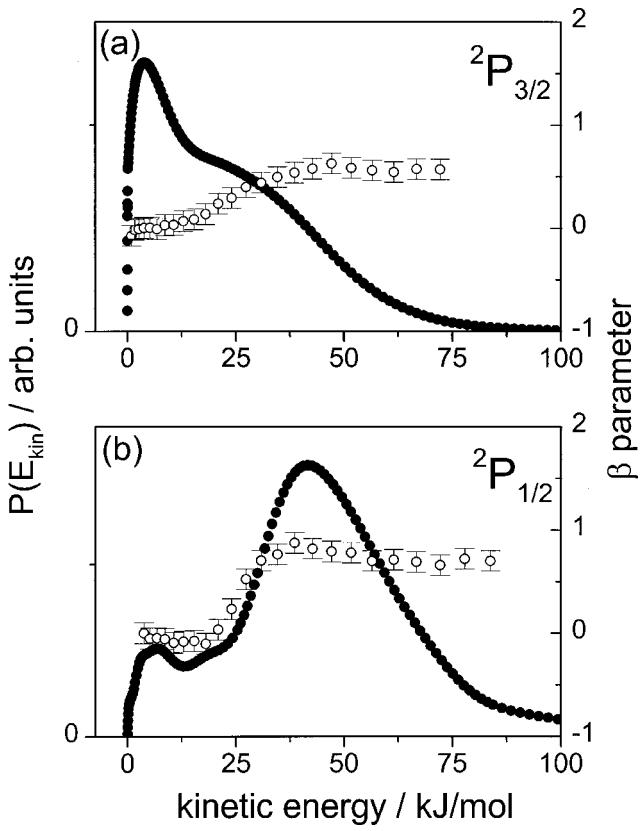

FIG. 3. Kinetic energy distribution for ground state $Cl(^2P_{3/2})$ (a) and excited state $Cl^*(^2P_{1/2})$ (b) atoms produced in the photodissociation of $COCl_2$ at 235 nm. The dependence of the β parameter on the Cl fragment kinetic energy (right scale) is shown by open circles with error bars. This 1D presentation is obtained via integration of the 3D data. Details of the respective high and low energy components of the bimodal distributions are listed in Table II.

The molecular channel cannot be observed directly in our experiments. Whether it exists or not can only be decided by monitoring the energetics of the CO molecule or by direct observation of the molecule chlorine fragment as nascent particle. The kinetic energy distribution of CO ($v=1$) molecules that was obtained via the $B\,^1\Sigma^+ \leftarrow X\,^1\Sigma^+$ transition at ~230.15 nm using (2+1) REMPI is shown in Fig. 4. Due to the maximal kinetic energies shown in Table I, it is concluded that only the CO fragments with higher kinetic energies than 120 kJ/mol can be released via the molecular channel. This leads to a contribution of the molecular channel of less than 20% to the CO ($v=1$) yield.

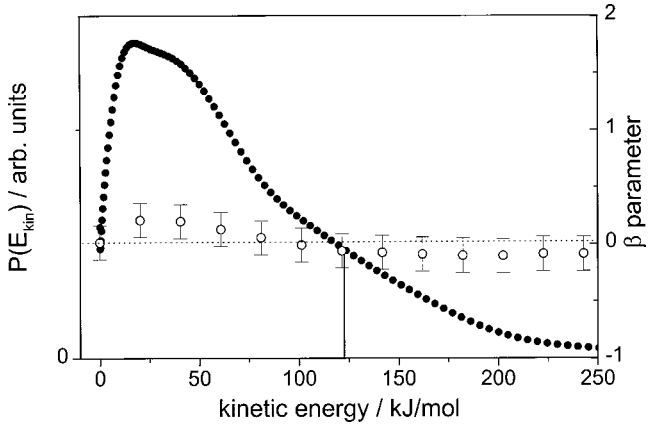

FIG. 4. Kinetic energy distribution for CO ($v=1$) produced in the photodissociation of $COCl_2$ at ~230.15 nm. The dependence of the β parameter on the CO fragment kinetic energy (right scale) is shown by open circles with error bars. The energetic threshold of the three-body decay channel is marked.

B. Spin–orbit state branching ratio

Scanning the laser over the two resonance transitions of Cl yielded Doppler profiles which were used for calculating the spin–orbital branching ratio. The measurements were repeated at different laser light intensities. Integrating the area S under the profiles results in a signal ratio $S(Cl^*)/S(Cl)$ of 0.27 ± 0.04. Taking the ratio of transition probabilities B of 1.06 (Ref. 27) into account we determined a Cl* yield $\phi(Cl^*)=0.22\pm0.03$ where ϕ is defined as the ratio of the number of excited state atoms $P(Cl^*)$ to the total number of chlorine atoms: $\phi(Cl^*)=P(Cl^*)/[P(Cl)+P(Cl^*)]$. This value agrees well with the previously determined value of $\phi(Cl^*)=0.15\pm0.03$, when the following two aspects are taken into account. Since no excited Cl* is produced within the experimental uncertainty of 5% at a dissociation wavelength of 248 nm,[15] it is concluded that the Cl* exit channel from the upper potential energy surface is opened when changing the dissociation wavelength from 248 to 235 nm. As Cl* was probed by 237.8 nm in the previous measurements, a smaller amount of Cl* is expected. And although the effect of ion-flyout was taken into account in the analysis of the former measurements, experimental inaccuracies as, e.g., the small size of the ionization volume lead to underestimating the contribution of fast particles. Ion-flyout occurs due to particles with slow velocity components v_z towards the detector and large velocity components v_y or v_x perpendicular to the detector so that these particles do not reach the detector inside its active radius. As Cl* in the spin–orbital excited state is preferentially released with high kinetic energies the total amount of Cl* could be slightly underestimated in the previous measurements.

C. Speed dependent anisotropy parameter β / velocity distribution

Previously, experiments were performed under conditions where the dissociation step was saturated.[10] Whereas state specific KED were determined and taken for a detailed discussion of the dissociation dynamics, the experimental observed fragment distribution was found to be independent of the polarization geometry and information about the β parameter could not be extracted. This does not mean, however, that the dissociation process itself is isotropic. As we are able to observe the three-dimensional (3D) momentum vector of a single reaction product we turned our attention to the observation of the speed dependent anisotropy parameter β. Experimental conditions were carefully chosen such that saturation of the dissociation did not occur.

In Fig. 3 the kinetic energy distributions and the kinetic energy dependent β parameters for Cl and Cl* are presented. This 1D presentation is obtained via integration of the 3D

TABLE II. Characteristic data describing the kinetic energy contributions of the Cl fragments in the $COCl_2$ dissociation. $\tilde{E}_{kin}$ describes the averaged kinetic energy in the two energy regions separately, whereas $\overline{E}_{kin}$ is the averaged value over the whole energy distribution. E_G is the center of the Gaussian.

Fragments		$\tilde{E}_{kin}$ (kJ/mol)	$\overline{E}_{kin}$ (kJ/mol)	Contribution (%)	E_G (kJ/mol)	β parameter
Cl	Slow	12	25	47	10	0
	Fast	42		31	36	0.7 ± 0.1
Cl*	Slow	9	46	3	10	0
	Fast	50		19	46	0.6 ± 0.1

data. Although both KED are bimodal, a remarkably different behavior of the two spin components with respect to their kinetic energy acquisition in the photodissociation is obvious. Cl in the electronic ground state is produced over the whole available energy range up to the calculated limit of 105 kJ/mol for the three-body decay. The bimodal character divides the energy distribution in two parts. Although the two parts are less clearly separated than in the case of Cl*, a limit between the fast and slow atoms of 25 ± 5 kJ/mol can be estimated. The peak of the slow Cl atom distribution is at 4 kJ/mol, whereas the peak for the fast atoms is at 30 kJ/mol. Cl* in the excited spin–orbit state is preferentially produced with large kinetic energies above 20 kJ/mol showing only a tail in the low energy region. The distributions for slow and fast Cl* atoms are clearly separated with a peak at 7 and 42 kJ/mol for slow and fast Cl*, respectively. Noteworthy is the kinetic energy dependence of the β parameter. In the case of particles with low kinetic energy the β parameter is about zero which means that the particles are isotropically distributed whereas in the region of high kinetic energy the β parameter increased to 0.6 ± 0.1 and 0.7 ± 0.1 for ground-state chlorine and spin–orbit excited Cl*, respectively. For Cl the increase happens smoothly starting at a kinetic energy value of 20 kJ/mol whereas for excited chlorine the increase of the β value happens rapidly at the same kinetic energy. Detailed information of the bimodal distributions for Cl and Cl* is given in Table II.

The fast chlorine atoms in both electronic states are preferentially released through an electronic transition with a positive β parameter. These values are close to the theoretical limit of 1.04 for the β parameter for instantaneous decay from the ground state geometry with a Cl–C–Cl bond angle of 111.3° if the nonplanar geometry of the excited state and the corresponding symmetry change from C_{2v} to C_S are considered. Hence the $A_2 \leftarrow A_1$ excitation becomes an optically allowed $A'' \leftarrow A'$ excitation with the transition dipole moment μ oriented parallel to the line connecting the two Cl atoms.

If only rotation[28] of the parent molecule is responsible for the reduction of the β parameter for ground and excited state chlorine, then lifetimes of $\tau = 230$ fs and 190 fs are estimated, respectively, based on the relationship

$$\tau = \frac{\eta}{\omega}, \tag{10}$$

where $\beta_{exp} = P_2(\eta)\beta^*$ and $\omega = \sqrt{\pi kT/2I}$.

Here η is the angle between the velocity vector that would result if the molecules were not rotating and the velocity vector that actually results, ω is the angular rotational frequency, β_{exp} the experimentally observed anisotropy parameter and β^* the theoretical limit. A molecular beam temperature of 8 K has been assumed. As the lifetime differences are due to the experimental inaccuracy in the β parameter measurement, a mean lifetime of 210 ± 20 fs is obtained. These small limiting lifetimes are a consequence of the large moments of inertia for the $COCl_2$ molecule leading to a fast loss of anisotropy due to molecule rotation. Under molecular beam conditions, in the case of Cl and Cl* with high kinetic energy a β value close to the limiting value is evidence of fast bond cleavage for the first step of the decay where one Cl or Cl* atom with high kinetic energy is released.

Taking the bimodal structure and the β parameter speed dependence into account, the existence of a sequential decay from the originally prepared excited state of the parent molecule is postulated. Fast Cl and Cl* atoms with a nonvanishing β parameter are released in the first step, and slow, predominantly ground state Cl atoms with an almost isotropic distribution are released in the second step.

With this picture one can divide the kinetic energy or velocity distribution in two parts. Hence, two overlapping Gaussians were fitted to the distributions, one describing the distribution of fast Cl atoms released in the first step with a β parameter of 0.65 and the second one describing the distribution of slow Cl atoms with a β parameter of zero released in the second dissociation step. The β value of 0.65 is taken as the mean experimental value observed for fast ground Cl and excited Cl* atoms. The velocity distributions were used for the fit procedure taking into account the branching ratios given in Table II. The centers of the Gaussians are at 750 m/s corresponding to 10 kJ/mol and 1440 m/s (36 kJ/mol) with widths of 1500 m/s (40 kJ/mol) and 1100 m/s (20 kJ/mol) for

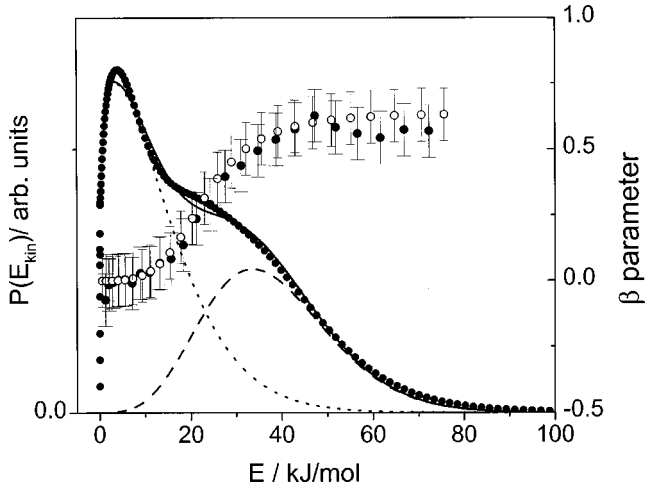

FIG. 5. Fit of the kinetic energy dependent β parameter (open circles) for the ground state $Cl(^2P_{3/2})$ to the experimentally observed data (solid circles) on the assumption that the decay proceeds via a sequential three-body decay. Two Gaussian were fitted to the bimodal velocity distribution, one describing the slow chlorine fragments with a β parameter of zero (dotted curve) and the other the fast chlorine fragments with a β parameter of 0.65 (dashed curve). The best-fit functions are shown in the graph. The asymmetry is due to the presentation of the Gaussian velocity fit in the energy domain.

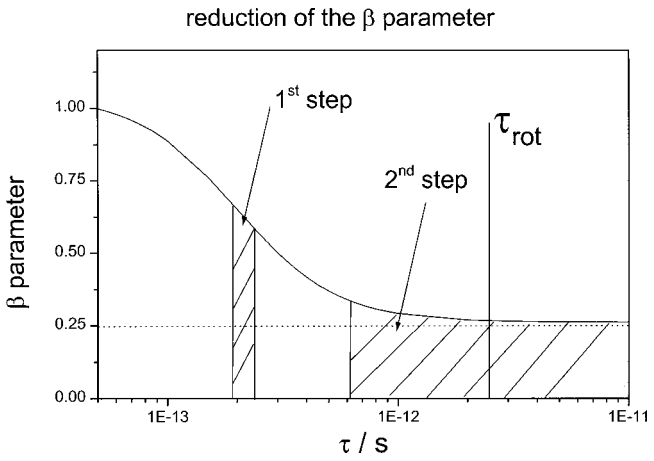

FIG. 6. The dependence of the observable β parameter on the lifetime of the intermediate $COCl_2^*$ or COCl* is clarified for the first and the second decay step, respectively. The observed time range of the first step is displayed as well as the estimated time range of the second step and the time of a rotational period. It can be seen that a slow asynchronous concerted decay mechanism cannot be distinguished from a pure sequential decay with certainty.

slow and fast Cl atoms, respectively. Considering these results, from the overlap one can calculate the theoretical β speed dependence of the ground state chlorine for a pure sequential decay. The obtained simulation is shown in Fig. 5. It is noteworthy that the two curves shown in the energy distribution in Fig. 5 are distorted due to the effect that the original Gaussians were fitted to the velocity distribution. The simulated β speed dependence is in very good agreement with the experimentally observed one. The small deviations are likely to be due to a small contribution of the synchronously concerted three-body decay. For the ground state Cl, the smooth transition from a vanishing β parameter to the maximum value is a consequence of the large contribution of slow ground state Cl compared to fast ground state Cl. Since the fit functions overlap in the medium energy range, the β parameter is accordingly reduced for ground state Cl, whereas for Cl* this effect is negligible due to the small contribution of slow excited state Cl*.

It is noteworthy that there is no suitable way to distinguish precisely between the pure sequential decay where the lifetime of the intermediate COCl* is longer than its rotational period and the very slow but still asynchronously concerted decay where the intermediate COCl* lives only slightly shorter than its rotational period. Figure 6 clarifies the issue. Theoretically even very slow fragmentations, $\eta \rightarrow \infty$, do not destroy the anisotropy of the fragments completely and therefore the β parameter is only reduced to 25% of its original value. Under assumption of a first-order decay which means that the lifetime distribution is described by a Poisson distribution, β is characterized[29] by

$$\beta = 2P_2(\cos\theta_t)\frac{1+\eta^2}{1+4\eta^2}, \tag{11}$$

where θ_t is the original angle between μ and v. The tangential velocity of Cl in the rotating parent can be neglected as the recoil velocity of Cl is high in comparison to the rotational velocity. As Fig. 6 shows, the photodissociation clearly proceeds in two steps, but whether the second decay: COCl*→CO+Cl proceeds late within or after a rotational period cannot be distinguished in our experiment. The reduction of the β parameter to a value below 25% of its original value indicates a transition of the $COCl_2$ molecule to a nonplanar geometry in the upper state, in accordance with considerations based on MO calculations.

The postulation of a sequential decay releasing the second Cl atom with an isotropic distribution agrees with the β dependence found for the CO molecule at ~230.15 nm, which is formed in the second step together with the slow component of the Cl atoms. The averaged value of the β parameter of 0.07 as shown in Fig. 4, confirms the isotropic nature of the second step in the sequential decay mechanism. Therefore it is assumed that predominantly the sequential decay takes place in the photodissociation at 235 nm which is in good agreement with former measurements.[9,10,30]

V. CONCLUSIONS

We report the direct observation of the 3D momentum vector of single Cl atoms in the uv photodissociation of phosgene as the first application of the recently developed 3D imaging technique. The previous results as there is the generation of chlorine in the $^2P_{3/2}$ electronic ground state as well as in the electronically excited $^2P_{1/2}$ state, the highly spin selective process with bimodal kinetic energy distribution and the overall decay mechanism as well as the branching ratios were confirmed. The anisotropy parameter β and its speed dependence were observed for the first time. A sudden change of the β parameter value at intermediate kinetic energy for both ground and excited state Cl and Cl* fragments is evidence of a stepwise, predominantly sequential process. The first bond cleavage produces fast Cl fragments in both spin–orbit states, the second bond cleavage generates slow Cl fragments preferentially in the electronic ground state. Products from the first step are distributed highly anisotropically which is evidence for a fast fragmentation in less than 210 fs on the originally accessed $^1A_2(A'')$ surface and an effective energy flow from the excited C–O bond to the C–Cl dissociation coordinate.

ACKNOWLEDGMENTS

The authors are greatly indebted to Dr. Uwe Titt and the Schmidt–Böcking group who strongly supported the electronic and experimental design and to Dr. Melanie Roth for her support and her continuous encouragement during the time of this work. These studies were generously supported by the Fonds der Chemischen Industrie and the Alexander von Humboldt foundation.

[1] E. W. G. Diau, C. Kotting, and A. H. Zewail, Phys. Chem. Chem. Phys. **2**, 273 (2001), and references therein.
[2] Q. Li, R. T. Carter, and J. R. Huber, Chem. Phys. Lett. **323**, 105 (2000).
[3] A. Furlan, H. A. Scheld, and J. R. Huber, J. Phys. Chem. A **104**, 1920 (2000).
[4] J. C. Owrutsky and A. P. Baronavski, J. Chem. Phys. **111**, 7329 (1999).
[5] R. J. Horwitz, J. S. Francisco, and J. A. Guest, J. Phys. Chem. A **101**, 1231 (1997).
[6] S. Deshmukh and W. P. Hess, J. Chem. Phys. **100**, 6429 (1994).

[7] S. Deshmukh, J. D. Myers, S. S. Xantheas, and W. P. Hess, J. Phys. Chem. **98**, 12535 (1994).
[8] C. Maul, C. Dietrich, T. Haas, and K.-H. Gericke, Phys. Chem. Chem. Phys. **1**, 1441 (1999).
[9] C. Maul, T. Haas, and K.-H. Gericke, J. Phys. Chem. A **101**, 6619 (1997).
[10] C. Maul, T. Haas, K.-H. Gericke, and F. J. Comes, J. Chem. Phys. **102**, 3238 (1995).
[11] C. Maul and K.-H. Gericke, Int. Rev. Phys. Chem. **16**, 1 (1997).
[12] C. Maul and K.-H. Gericke, J. Phys. Chem. A **104**, 2531 (2000).
[13] D. C. Moule and P. D. Foo, J. Chem. Phys. **55**, 1262 (1971).
[14] H. Okabe, A. H. Laufer, and J. J. Ball, J. Chem. Phys. **55**, 373 (1971).
[15] A. Chichinin, Chem. Phys. Lett. **209**, 459 (1993).
[16] A. Chichinin, T. Einfeld, C. Maul, and K.-H. Gericke, Rev. Sci. Instr. **73** (in press).
[17] S. E. Sobottka and M. B. Williams, IEEE Trans. Nucl. Sci. **35**, 348 (1988).
[18] O. Jarutzki, V. Mergel, K. Ullmann-Pfleger, L. Spielberger, U. Meyer, R. Dörner, and H. Schmidt-Böcking, *Proceedings in Imaging Spectrometry IV, San Diego, California* (1998).
[19] M. Lampton, O. Siegmund, and R. Raffanti, Rev. Sci. Instrum. **58**, 2298 (1987).
[20] J. Danielak, U. Domin, R. Kepa, M. Rytel, and M. Zachwieja, J. Mol. Spectrosc. **181**, 394 (1997).
[21] D. Ascenzi, P. M. Regan, and A. J. Orr-Ewing, Chem. Phys. Lett. **310**, 477 (1999).
[22] S.Arepalli, N. Presser, D. Robie, and R. J. Gordon, Chem. Phys. Lett. **118**, 88 (1985).
[23] T. Ishiwata, A. Ishiguro, and K. Obi, J. Mol. Spectrosc. **147**, 300 (1991).
[24] Y. Matsumi, K. Tonokura, and M. Kawasaki, J. Chem. Phys. **97**, 1065 (1992).
[25] P. C. Samartzis, I. Sakellariou, Th. Gougousi, and Th. N. Kitsopoulos, J. Chem. Phys. **107**, 43 (1997).
[26] M. W. Chase, *NIST-JANAF, Thermochemical Tables*, fourth ed. [J. Phys. Chem. Ref. Data, Monograph 9, Parts I+II (1998)].
[27] P. M. Regan, S. R. Langfold, D. Ascenzi, P. A. Cook, A. J. Orr-Ewing, and M. N. R. Ashfold, Phys. Chem. Chem. Phys. **1**, 3247 (1999).
[28] G. E. Busch and K. R. Wilson, J. Chem. Phys. **56**, 3638 (1972).
[29] K.-H. Gericke, Photodissoziationsdynamik kleiner Moleküle, habilitation thesis, Frankfurt a. M., 1990.
[30] M. H. Wijnen, J. Am. Chem. Soc. **83**, 3014 (1961).